Research on the Strengthening Mechanism of MWCNTs-Cu_f Composite Interlayer for Si_3N_4/TC4 Brazed Joints

An innovative approach using MWCNTs-Cu_f composite interlayer to reduce residual stress and enhance Si_3N_4/TC4 joint strength

BY B. LI, L. CAO, Q. LIU, J. GAO, AND R. LI

Abstract

With the rapid development of aerospace technology, the high-quality brazing connection between Si_3N_4 ceramic and TC4 titanium alloy has become a key factor in advancing the development of aircraft antenna covers. To improve the mechanical strength of the joints, this study used the electrophoretic deposition method to prepare a multi-walled carbon nanotubes-foam copper (MWCNTs-Cu_f) composite interlayer and selected the optimal deposition parameters. The most suitable brazing parameters under this interlayer were also determined. The joints' formation mechanism and fracture mode were revealed to elucidate the synergistic strengthening mechanism of the composite interlayer. The results showed that MWCNTs, based on their phase characteristics, produced high-density dislocations and fine crystal strengthening effects during the brazing cooling process. This effectively resisted the corrosion of the brazing material on the foam copper (Cu_f), protected the integrity of the foam copper framework, and exerted the excellent plastic deformation ability of foam copper (Cu_f). It reduced the residual stress in the joints, resulting in the highest shear strength of the MWCNTs-Cu_f composite interlayer, reaching 96.23 MPa. Compared with only adding Ag-Cu-Ti active brazing filler metal and adding ordinary foam copper interlayer, the shear strength increased by 78.2% and 44.7%, respectively.

Keywords

- Si_3N_4/TC4
- MWCNTs-Cu_f Composite Interlayer
- Shear Strength
- Fracture Mode
- Strengthening Mechanism

Introduction

Si_3N_4 ceramics have emerged as a cutting-edge material for missile radomes because of their superior wave transmission capabilities and mechanical strength (Refs. 1–3). However, the inherent processing challenges of Si_3N_4 necessitate using a metal connecting ring to join the radome with the missile structure. TC4 titanium alloy, notable for its high specific strength, corrosion resistance, and exceptional overall properties, is poised to be the preferred choice over Invar alloy for this purpose (Ref. 4) Consequently, a high-quality bond between Si_3N_4 ceramics and TC4 titanium alloy is pivotal for advancing the development of aircraft radomes. Compared with the problems of high cost and stress concentration caused by cementation (Ref. 5) and mechanical connection (Refs. 6–8), brazing has gradually become the most widely used connection mode in ceramic-metal connections (Ref. 9) because of its advantages of less damage to the base metal, high precision, and low production cost. However, due to the significant differences in chemical bond types, thermal expansion coefficients, and elastic modulus between ceramics and metals, there are two difficulties in realizing high-quality brazing between them: the wettability of brazing filler metals to ceramics is poor, and it is difficult for brazing filler metals to spread on ceramic substrates after being heated and melted; The residual stress produced by a brazed joint greatly affects joint strength (Refs. 10–12). One strategy to mitigate the

https://doi.org/10.29391/2025.104.003

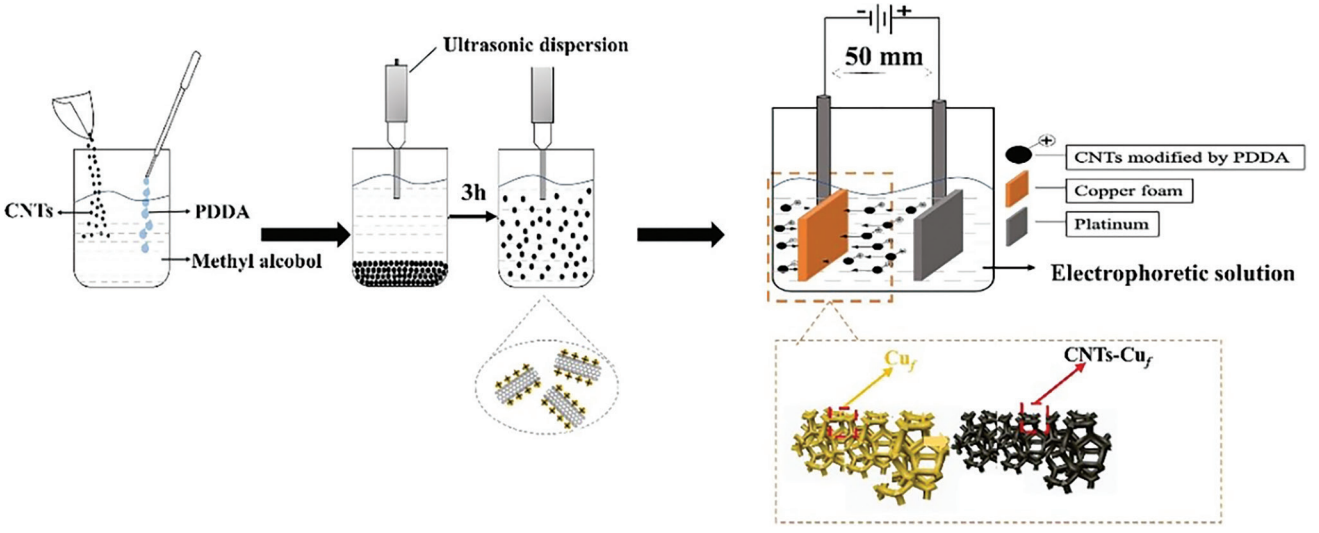

Fig. 1 — Schematic diagram of the electrophoretic deposition process.

residual stress in brazing involves incorporating reinforcement phases through direct mechanical ball milling or the in-situ reaction within traditional brazing filler metal to fine tune the thermal expansion compatibility with the base metal (Refs. 13–15). Song et al. (Ref. 16) integrated Si_3N_4 particles into the Ag-Cu-Ti brazing filler metal. This lessened the thermal expansion and modulus disparities between Si_3N_4 and the TiAl matrix, improving joint strength. Bridges et al. (Ref. 17) investigated the wetting and diffusion behavior of different shapes of silver nanomaterials (silver nanoparticles and silver nanowires) as filler materials during the laser brazing process of Inconel 718 and their influence on the strength of brazed joints. In addition, they achieved high joint strength of up to 243 MPa by synthesizing different nickel nanoparticles for Inconel 718 brazing joints. Based on this, they also elucidated the quantitative and qualitative influences of heating rate on microstructure and mechanical properties (Ref. 18). Alternatively, introducing an intermediate layer to create a composite brazing filler metal structure during brazing demonstrates great potential in improving bond performance (Refs. 19–21). Sun et al. (Ref. 22) utilized a W foil interlayer with Ag-Cu-Ti brazing filler metal to address the thermal expansion mismatch between Invar alloy and SiO_2 ceramics, preventing the formation of brittle Fe_2Ti and Ni_3Ti compounds, resulting in a 1.75-fold increase in shear strength. Brochu et al. (Ref. 23) selectively employed a Cu interlayer when brazing Si_3N_4 ceramics to FA-129 using 75Cu25Ti brazing filler metal, leveraging Cu's ductility to absorb residual stresses. Shirzadi et al. (Ref. 24) brazed Al_2O_3 ceramics to 316L stainless steel using a foam stainless steel interlayer and Ag-Cu-Ti brazing filler metal, exploring how the thickness of the foam interlayer impacts the joint's mechanical properties. Despite these advancements in strength optimization, relying solely on reinforcement methods such as adding nanoparticles or constructing a single intermediate layer does not yield the desired outcome in heterogeneous material bonding. In the composite brazing method, it is challenging to determine the optimal amount of reinforcement phase addition for improving the joint structure and performance. An insufficient reinforcement phase may not effectively reduce the thermal expansion coefficient of the brazing material. At the same time, excessive amounts can lead to phenomena such as accumulation in the brazing layer, resulting in decreased joint performance. In the intermediate layer method, new interfaces are formed at the joint, which is prone to cracks and voids due to differential properties with the brazing material and base metal. More importantly, they have not systematically elucidated dissimilar materials' reinforcement mechanisms and fracture modes.

To enhance the bonding quality between Si_3N_4 ceramics and TC4 titanium alloy, this study fully utilized the characteristics of multi-walled carbon nanotubes (MWCNTs), such as high strength and modulus and directed high thermal conductivity (Refs. 25–27), combined with foam copper, which possesses good ductility (Ref. 28). The electrophoretic deposition technique synthesized a multi-walled carbon nanotubes-foam copper (MWCNTs-Cu_f) composite interlayer. Comparative experiments led to the determination of optimal deposition parameters to achieve a uniform interlayer. The joint with the utmost strength was achieved by modifying the brazing temperature and dwell time. Additionally, analyses of the microstructure, elemental distribution, and fracture morphologies revealed three distinct fracture modes of the joint. The study sheds light on the collaborative reinforcement mechanism by which the MWCNTs-Cu_f composite interlayer fortifies the brazed joints, affirming the composite's reinforcing impact.

Experimental Procedures

The experimental base materials comprised MWCNTs sourced from Pioneer Nanomaterials Technology Co., Ltd., featuring diameters between 5–15 nm, lengths spanning 10–30 μm, and a purity exceeding 95%. The Ti-6Al-4V alloy, commonly recognized as TC4 titanium alloy, consisting pri-

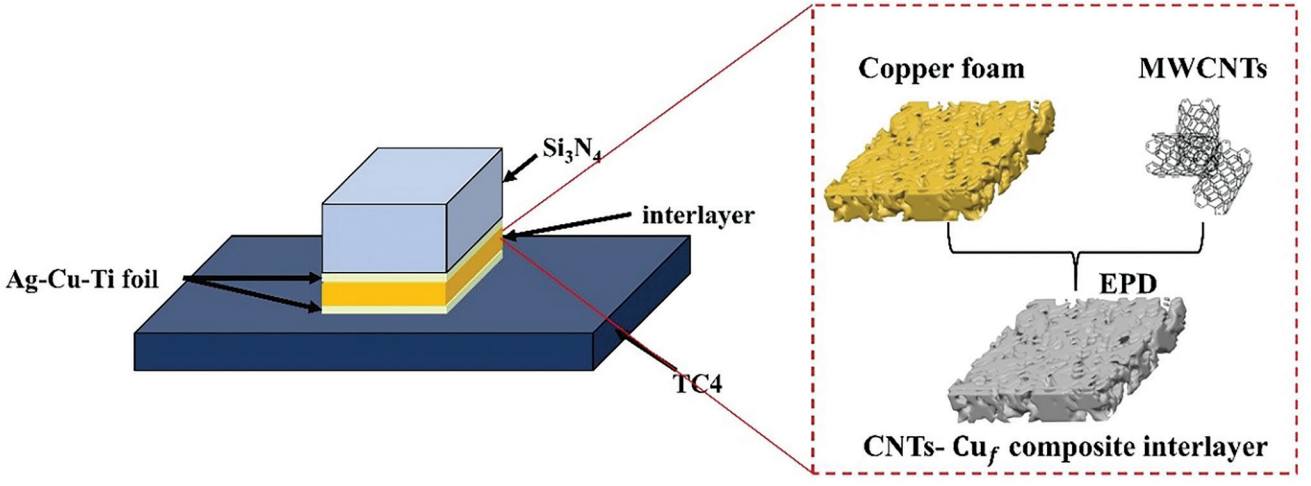

Fig. 2 — Schematic diagram of assembly form of sample to be brazed.

marily of α and β phases, was procured commercially. Si_3N_4 ceramics were obtained from Hyde Precision Ceramics, measuring 5 × 5 × 5 mm^3, with a 3.2 g/cm^3 density and a coefficient of thermal expansion (CTE) of 3.2 × 10^{-6}/K.

The foam copper was sectioned into 5 × 5 × 1 mm^3 pieces, followed by degreasing in a 1:1 volumetric mixture of acetone and absolute ethanol for 30 min to eliminate any oil residues. Subsequently, the foam underwent a 30-min immersion in a 6 mol/L hydrochloric acid (HCl) solution to remove surface oxides. The preparation of the electrolyte involved weighing 30 mg of acid-cleaned MWCNTs and 60 mg of dimethyl diallyl ammonium chloride (PDDA), which were then introduced into 100 ml of methanol, stirred thoroughly, and dispersed via ultrasonic agitation for three hours.

The MWCNTs-Cu_f composite interlayer fabrication employed the electrophoretic deposition technique to embed MWCNTs within the copper foam, as depicted in Fig. 1. The copper foam served as the cathode for the electrophoretic deposition process, with platinum acting as the anode. The plates were positioned with a fixed separation of 50 mm.

The TC4 titanium alloy was sectioned into specimens of dimensions 20 × 10 × 3 mm^3 and 10 × 10 × 3 mm^3 using a wire-cutting machine followed by sanding to achieve a smooth surface. Similarly, Si_3N_4 ceramic samples were sliced to 5 × 5 × 5 mm^3 using a diamond wire saw and subsequently polished to remove any surface imperfections. The Ag-Cu-Ti brazing foil and the MWCNTs-Cu_f composite interlayer were trimmed to 5 × 5 mm square pieces. Before brazing, the base metals, brazing foil, and interlayer were cleansed in an acetone solution for 15 min. This process was repeated three times to ensure the removal of any surface contaminants.

The prepared MWCNTs- Cu_f composite interlayers were an intermediary in brazing Si_3N_4 ceramics to TC4 titanium alloy. The base metal, brazing filler metal, and interlayer were stacked in a sandwich configuration and secured using an adhesive, as depicted in Fig. 2. To ensure optimal contact and adherence during the brazing process, the assembled stack was placed into a custom-designed metal fixture, where pressure was applied to maintain tight interfacing between the brazing filler metal and the base metals.

The TL1200 vacuum tube furnace was utilized for the brazing process, with a maximum operational temperature cap of 1200°C. Vacuum levels within the tube during the heating cycle were maintained between 1 × 10^{-3} and 5 × 10^{-3} Pa, achieved by sequential usage of a mechanical pump followed by a molecular pump. Initially, the tube furnace was ramped up to 300°C at a rate of 10°C/min and held at this temperature for 30 min to ensure complete volatilization of the binder used in sample assembly. The temperature was then increased to the target value at a rate of 6°C/min and maintained for a designated duration. This study explored how variations in brazing temperature and hold time influenced the strength of the joint. During the cooling phase, the furnace's decrement rate was regulated at 5°C/min down to a temperature of 400°C. This controlled rate of cooling was intended to avert potential thermal deformation and the generation of residual stress that could arise from rapid temperature change. After reaching 400°C, the assembly was allowed to cool to ambient temperature within the furnace's environment.

Results and Discussion

Morphology and Characterization of Intermediate Layer

Given the nanoscale dimensions and significant aspect ratio of MWCNTs, they tend to tangle owing to van der Waals forces within a solution, making their even distribution in an electrolyte a challenge. To address this, an acid washing process was applied to not only cleanse the surface of oily contaminants but also to introduce hydroxyl functional groups. When ionized in the solution, these functional groups endow MWCNTs with a negative charge, enhancing the electrostatic repulsion between the individual MWCNTs (Ref. 29). Nonetheless, acid washing alone does not suffice

to induce a directional movement of MWCNTs under an electric field; the addition of electrolyte ions is necessary. To this end, dimethyl diallyl ammonium chloride (PDDA) was incorporated at a mass ratio of 2:1 concerning MWCNTs to facilitate surface modification through ion introduction. The process harnesses π-π bonding (Ref. 30) through conjugation, enabling PDDA to attach to the MWCNTs' exterior, consequently imparting a positive charge to them. Post ultrasonic agitation, this treatment yielded a stable dispersion of MWCNTs within methanol. This stable dispersion was subsequently deposited onto the foam copper to fabricate the composite interlayer.

To achieve an optimally uniform deposition morphology, various experimental parameters were systematically varied, as illustrated in Fig. 3. At excessively low deposition voltages, abbreviated deposition durations, and minimal MWCNT concentrations, the surface of the foam copper was coated with a mere single layer of MWCNTs. This suboptimal coverage failed to harness the potential reinforcement properties of MWCNTs for subsequent brazing tests. Conversely, when deposition times are unduly prolonged and MWCNT concentrations are heightened, the predicament of MWCNT agglomeration arises, which may culminate in localized stress concentrations, undermining the strength of the resultant brazed joints. Through comparative assessment of disparate deposition voltages (80 V, 100 V, 120 V), varying deposition times (10 min, 20 min, 30 min), and distinct MWCNTs concentrations (0.2 mg/mL, 0.3 mg/mL, 0.4 mg/mL), the ideal set of parameters was pinpointed to attain a uniform interlayer morphology, specifically a voltage setting of 120 V, a deposition time of 20 min, and a MWCNTs concentration of 0.3 mg/mL. In addition, during the acid treatment process, acidic solutions can chemically corrode the surface of MWCNTs, leading to the formation of surface irregularities or corrosion pits. Subsequently, when using PDDA to modify the surface of carbon nanotubes to form functionalized carbon nanotubes, the surface is decorated by PDDA, and the uneven modification behavior inevitably results in surface roughening of the MWCNTs. This phenomenon can be observed in Fig. 3.

Effect of Composite Interlayer on Joint Strength under Different Brazing Temperatures and Holding Time

Brazing temperature and holding time also have a great influence on joint morphology, thus affecting joint strength. Fig. 4 shows the interface morphology of brazed Si_3N_4 ceramics and TC4 titanium alloy with a MWCNTs-Cu_f composite interlayer at different temperatures. Fig. 5 shows the interface morphology of brazed Si_3N_4 ceramics and TC4 titanium alloy with a MWCNTs-Cu_f composite interlayer under different holding times. When the brazing temperature was too low,

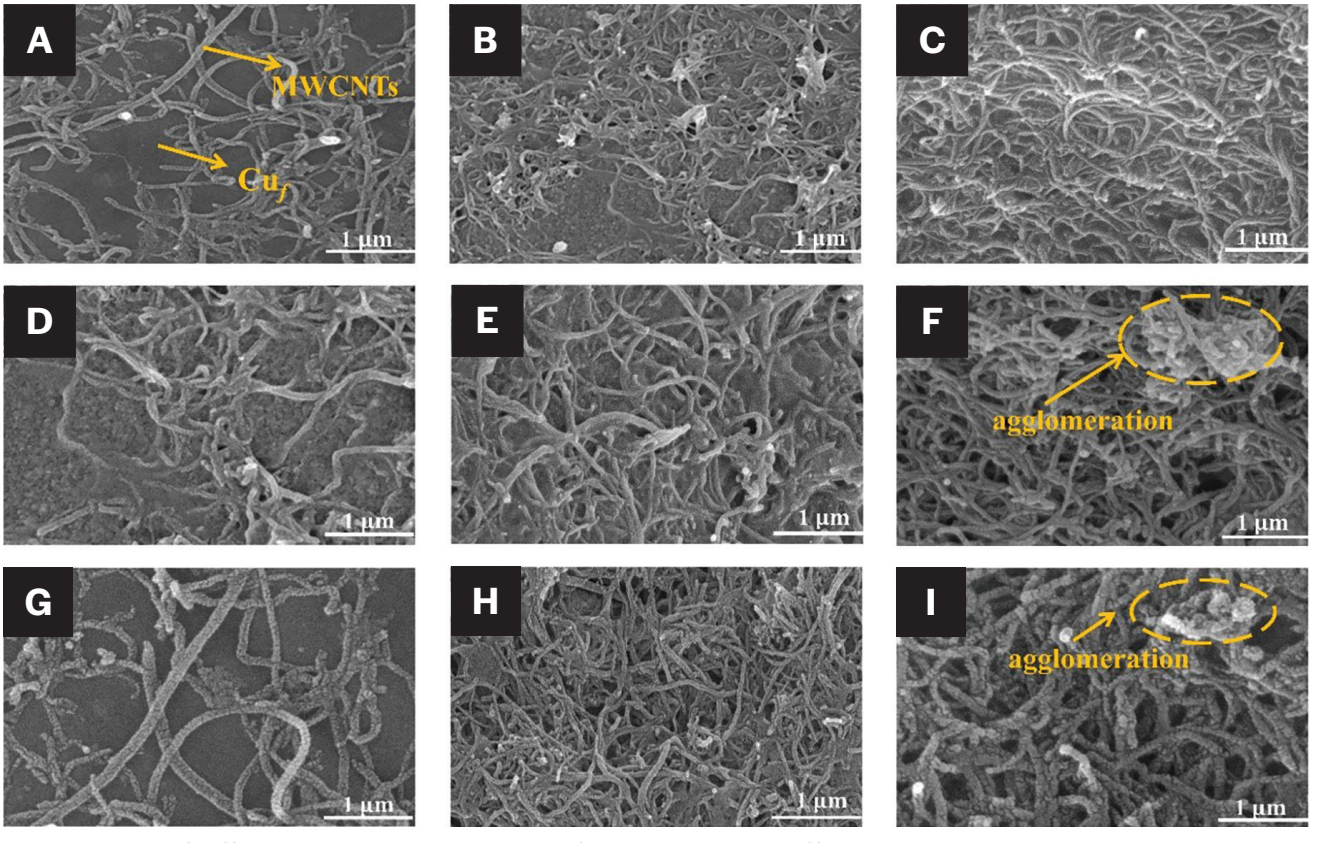

Fig. 3 — SEM of different processes: (A–C) SEM of interlayer under different deposition voltages: A — 80 V; B — 100 V; C — 120 V; (D–F) SEM at different deposition times: D — 10 min; E — 20 min; F — 30 min; (G–I) SEM of interlayer under different MWCNTs: G — 0.2 mg/mL; H — 0.3 mg/mL; I — 0.4 mg/ml.

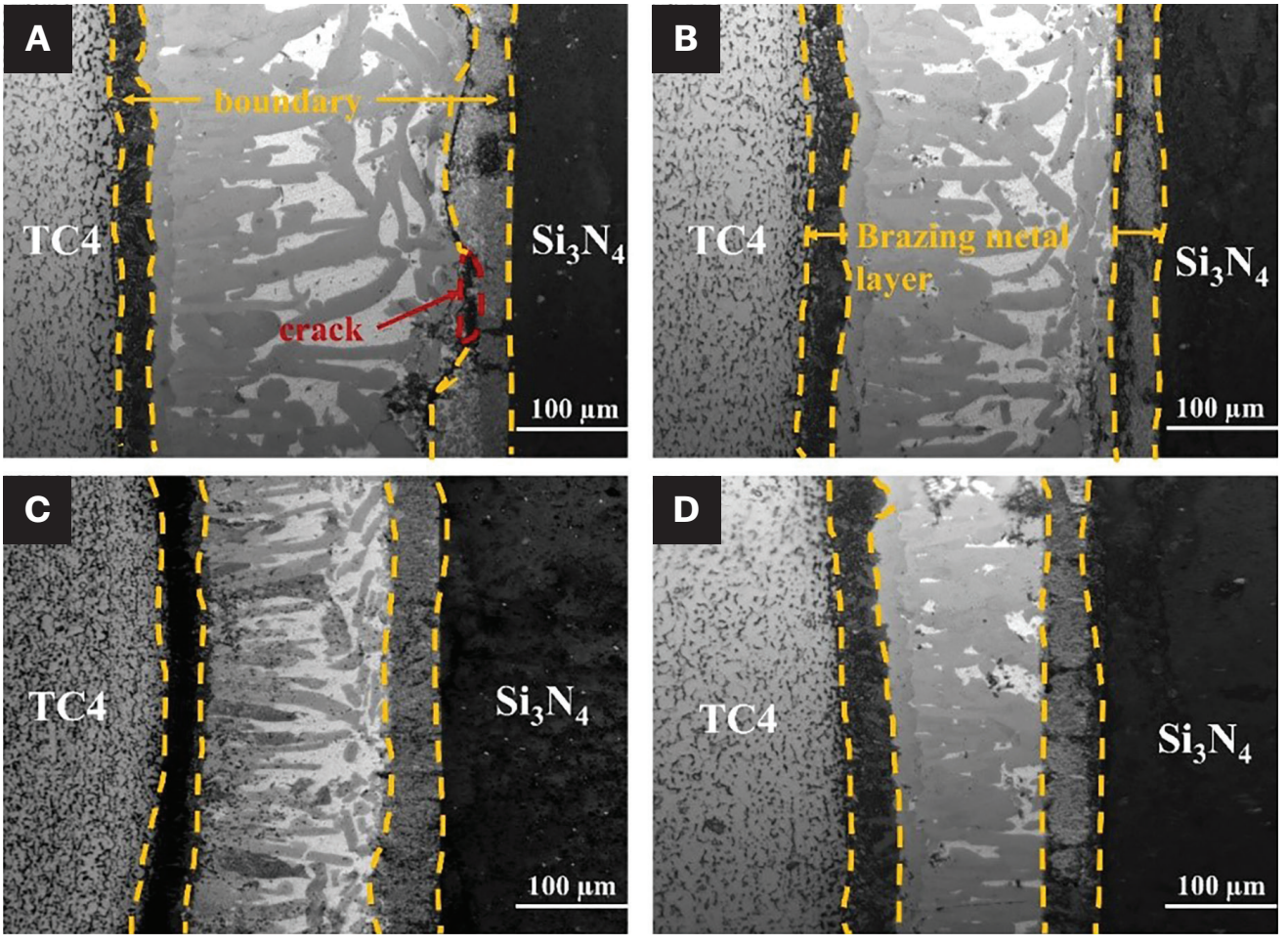

Fig. 4 — Effect of different brazing temperatures on microstructure and morphology of joint interface (holding time 10 min): A — 820°C; B — 850°C; C — 880°C; D — 910°C.

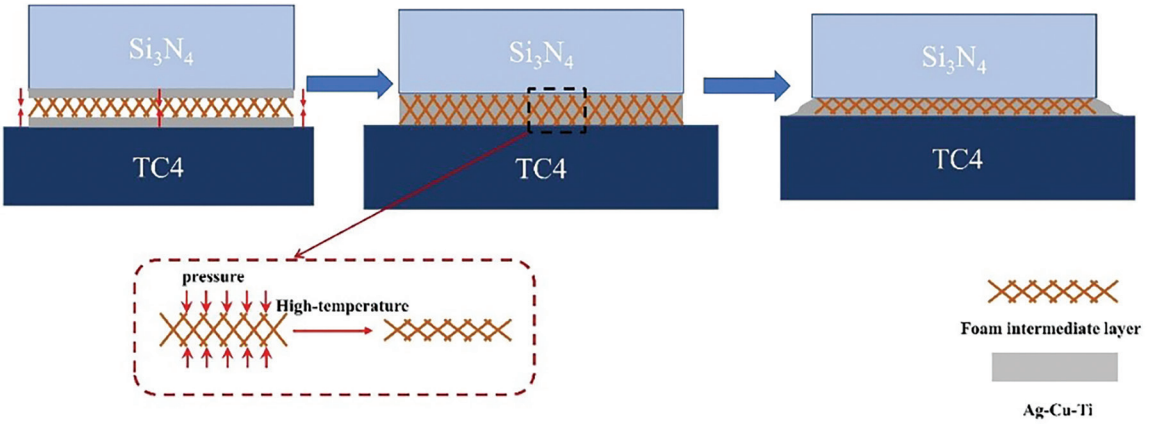

Fig. 5 — The mechanism of softening and collapse of foam copper.

the fluidity of brazing filler metal was poor and could not completely flow into and fill the foam copper with porous structure, resulting in pores, which reduced the actual contact area and produced local stress concentration. Cracks initiated and developed here, which affected the joint strength. The shear strength of the joint was 75.64 Mpa. When the brazing temperature was slightly higher than the melting point of Ag-Cu-Ti, the pores of MWCNTs-Cu_f were filled by brazing filler metal, the whole brazing layer remained compact and continuous, and the foam copper skeleton further

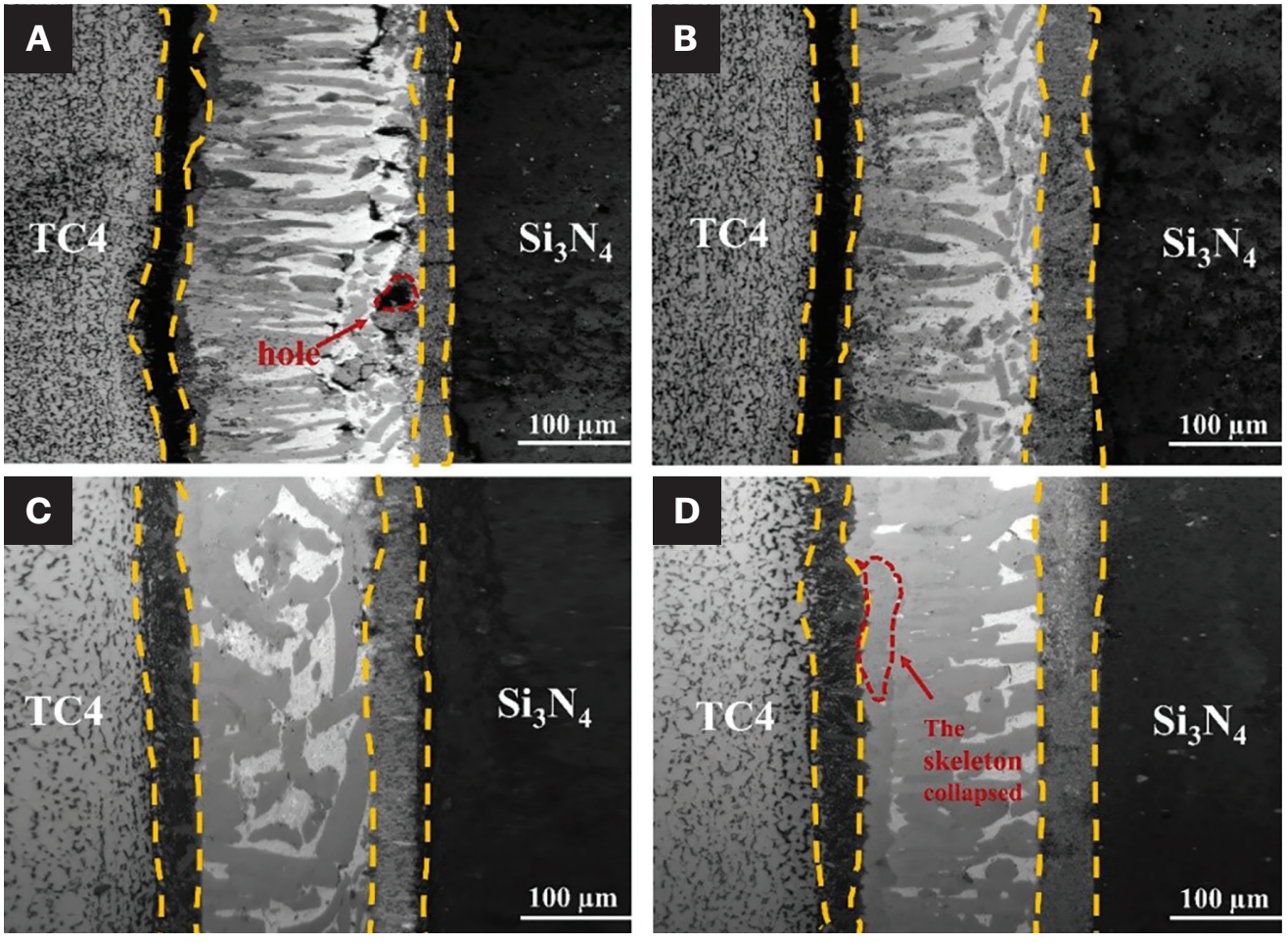

Fig. 6 — Effect of different holding times on microstructure and morphology of joint interface (brazing temperature 880°C): A — 5 min; B — 10 min; C — 15 min; D — 20 min.

softened. However, due to the existence of MWCNTs, the collapse of copper foam was hindered to a certain extent, so q was uniformly distributed in the brazing layer. At this time, the shear strength of the joint reached the maximum value of 96.23 MPa. Under the same process parameters, the shear strength of the joint without interlayer was only 54.24 MPa, and that of the joint with only common foam copper was 66.72 MPa. (Compared with the above two joints, the shear strength of the joint with MWCNTs-Cu_f composite interlayer was increased by 77% and 44%, respectively). When the brazing temperature was too high, the copper-based solid solution (Cu (s, s)) was distributed in the brazing seam in the form of blocks, which made the protection of MWCNTs to copper foam beyond the bearable range. At high temperatures, copper foam completely contacts with molten brazing filler metal, which leads to excessive softening and collapse and finally leads to the residual stress in the joint not being alleviated, resulting in a significant decrease in shear strength of the joint to 63.17 MPa. The reason for the collapse is that copper is a soft metal with good ductility and plastic deformation ability. Pure copper undergoes compressive deformation at high temperatures, and its peak stress decreases with increasing temperature. This indicates that as the brazing temperature increases, copper is more prone to plastic deformation. Foam copper, as a porous scaffold structure, has greater deformation capability compared to bulk copper, and its high-temperature softening phenomenon is more pronounced. Therefore, with the increase of brazing temperature or prolongation of insulation time, the degree of plastic deformation of the MWCNTs-Cu_f composite intermediate layer increases continuously while reacting with the brazing filler metal, and in actual brazing processes, to ensure tight contact between the brazing filler metal and the substrate without movement, pressure is usually applied to the top of the brazed sample. Considering the above reasons, the deformation softening of foam copper gradually intensifies, and collapse may even occur under excessively high brazing temperatures or prolonged insulation times, as shown in Fig. 5. The holding time also affects the flow of brazing filler metal. When the holding time was 5 min, a small number of holes appeared in the brazing seam. Because the holding time was too short, the brazing filler metal in the molten state began to cool down and solidify before filling the pores of the MWCNTs-Cu_f composite interlayer, the interfacial reaction layer was very thin, the load could not be effectively transmitted, and the shear strength of the joint was low, only 83.48 MPa. With the prolongation of holding time, Ag-Cu-Ti active brazing filler metal had enough time

to flow into the MWCNTs-Cu_f skeleton and fill its pores, and the pores disappeared. Therefore, when the holding time was 10 min and 15 min, the whole brazed layer was continuous and intact, and the shear strength of the brazed joint was 96.23 MPa and 91.63 MPa, respectively. Under the above two conditions, MWCNTs always play an important role in preventing copper foam from being eroded by Ti in brazing filler metal. It can be observed from Figs. 6B and 6C that Cu (s, s) kept a uniform distribution, while when the holding time was extended to 20 min, some structures of MWCNTs collapsed at high temperatures for a long time, which seriously affected their properties, as shown in Fig. 6D. At the same time, the copper foam completely exposed to brazing filler metal softened seriously at continuous high temperature, and Cu (s, s) agglomerated and existed on the TC4 side in block form. The residual stress caused by the difference in thermal expansion coefficient of the joint could not be alleviated, and the shear strength of the joint was 86.47 MPa. On the whole, the change of holding time had little effect on the shear strength of brazed joints, as shown in Fig. 7B.

Subsequent analysis of joint element distribution with the improved parameters demonstrated that the brazing filler metal exhibited robust continuity and lacked apparent cracks, as evidenced by Fig. 8. The joint can be segregated into three distinct zones: Zone I is the could reaction layer adjacent to the TC4 titanium alloy; Zone II represents the brazing seam's core layer, while Zone III primarily comprises the Si_3N_4 ceramic interface reaction layer. These three zones were magnified, and EDS energy spectrum analysis was performed on different phases, with the outcomes presented in Table 1. Fig. 9 illustrates the microstructure of the three zones in greater detail. Per the EDS findings, Point A predominantly consists of Ti, Al, and V, with Ti present in the highest concentration, derived principally through the dissolution and diffusion of TC4. As for Points B through E, their composition is chiefly of Ti and Cu, albeit in varying ratios, suggesting the formation of a Ti-Cu intermetallic compound. Detailed element composition analysis of each point in Table 1 allows for delineating the reaction layer in Zone I as TC4/diffusion layer/Ti_2Cu/TiCu/Ti_3Cu_4/$TiCu_4$. Zone II is identified as the brazing layer, where a substantially dispersed, gray phase F predominantly consists of copper, signifying a copper-based solid solution (Cu (s, s)) resulting from the high-temperature softening and cooling solidification of foam copper. The lustrous white phase G is constituted of a silver-based solid solution (Ag (s, s)) and a minute quantity of the black J phase, consisting of Ti and C with an approximate 1:1 composition ratio, indicating the formation of TiC through the reaction between the brazing filler metal and TC4 substrate's Ti, as well as MWCNTs within the MWCNTs-Cu_f composite interlayer. Moreover, the brazing layer contains a eutectic structure, H. EDS data reveals an Ag-to-Cu ratio closely approximating 3:2, deduced as an Ag-Cu eutectic structure based on its morphological features. Zone III is the Si_3N_4 ceramic interface reaction layer, characterized by a predominance of Ti, N, and Si elements. It is inferred that Ti from the brazing filler metal reacts with the Si_3N_4 ceramic substrate upon diffusion, eventually forming a TiN + Ti_5Si_3 interface reaction layer, in concurrence with results obtained from Si_3N_4 ceramic brazing experiments using Ti-based brazing filler metal (Refs. 31, 32). Consequently, the reaction layer in Zone III is Ti_5Si_3/TiN/Si_3N_4. The copper diffusion and the erosive action of Ti flux on the copper foam are hypothesized to disrupt the foam's integrity, and the brittle phase precipitated by diffusion, such as TiC, may induce joint cracks and diminish structural fidelity. Concurrently, the reaction layer's thickness directly influences the brazing filler metal bead's breadth and engenders disparate residual stresses. Subsequently, we shall elucidate the specific mechanism by which MWCNTs impede elemental diffusion and employ finite element simulation to appraise the impact of brazing filler metal thickness on residual stress.

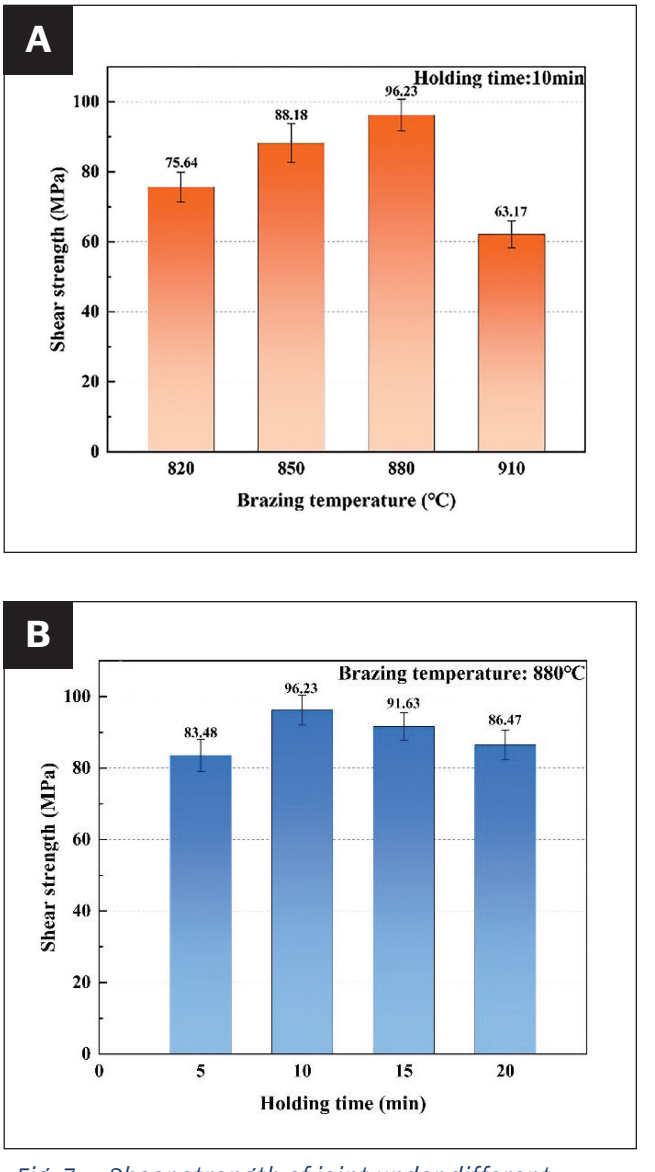

Fig. 7 — Shear strength of joint under different brazing parameters: A — Holding time 10 min and different brazing temperatures; B — brazing temperature 880°C and different holding times.

Formation Mechanism of Joint Morphology and Fracture Mode of Joint

Through the analysis of Table 1 and the EDS results, the formation mechanism of the overall morphology of the joint can be summarized as shown in Fig. 10. Fig. 10A shows the joint state at 25°C ≤ T ≤ 780°C (780°C is the melting point of Ag-Cu-Ti brazing filler metal). With the increase in temperature, the brazing filler metal kept close contact with the composite interlayer and brazing base metal under the pressure of Si_3N_4 ceramics. Atoms began to move violently, but they did not interact with the base metal, and the brazing filler metal remained solid because it had not reached its melting point. Fig. 10B shows that when the temperature reached the melting point of the brazing filler metal, the molten brazing filler metal began to spread between the base metals and immerse into the MWCNTs-Cu_f composite interlayer. Under the action of high-temperature liquid brazing filler metal, some of the base metals on both sides began to dissolve. Ti diffused in the direction of Si_3N_4 ceramics, while Cu diffused in the direction of the TC4 base metal. At the same time, many Ti elements and some Al elements in TC4 dissolved and diffused in the direction of the brazing filler metal, and the MWCNTs-Cu_f composite interlayer softened due to high temperature. Fig. 10C shows the holding stage, in which a large number of dissolved Ti elements and a small amount of Al elements attached to the TC4 side to form a diffusion layer, and Ti elements with the largest proportion reacted with Cu elements in the brazing filler metal to form TiCu compounds. Ti reacted with Si_3N_4 particles on the ceramic side to form TiN and Si, while the newly formed Si reacted with Ti to form Ti_5Si_3, forming a TiN + Ti_5Si_3 reactive layer on the ceramic side. Due to the protection of MWCNTs deposited on the surface, the diffusion of copper in copper foam was hindered, and the integrity of the foam copper structure was ensured. However, MWCNTs will adsorb a small amount of diffused Ti to the surface and react with it to form TiC. Fig. 10D shows the cooling stage. With the decrease in temperature and the consumption of Ti elements, Ti_3Cu_4/$TiCu_4$ reaction layers began to be formed in turn on the TC4 side. At the same time, Ti elements dissolved and diffused in TC4 have difficulty reaching equilibrium with the formed TiCu phase, and the solid solubility will decrease with the decrease of temperature, providing more nucleation driving force and forming Ti_2Cu compounds. Therefore, the final reaction layer on the TC4 side was composed of TC4/Ti_2Cu/TiCu/Ti_3Cu_4/$TiCu_4$. Ti and Si_3N_4 on the ceramic side were cooled and solidified by mutual reaction, and finally, Si_3N_4/TiN/Ti_5Si_3 was formed. The Cu foam maintained its skeleton structure after softening under the action of MWCNTs and dispersed in the brazing layer as a copper-based solid solution after

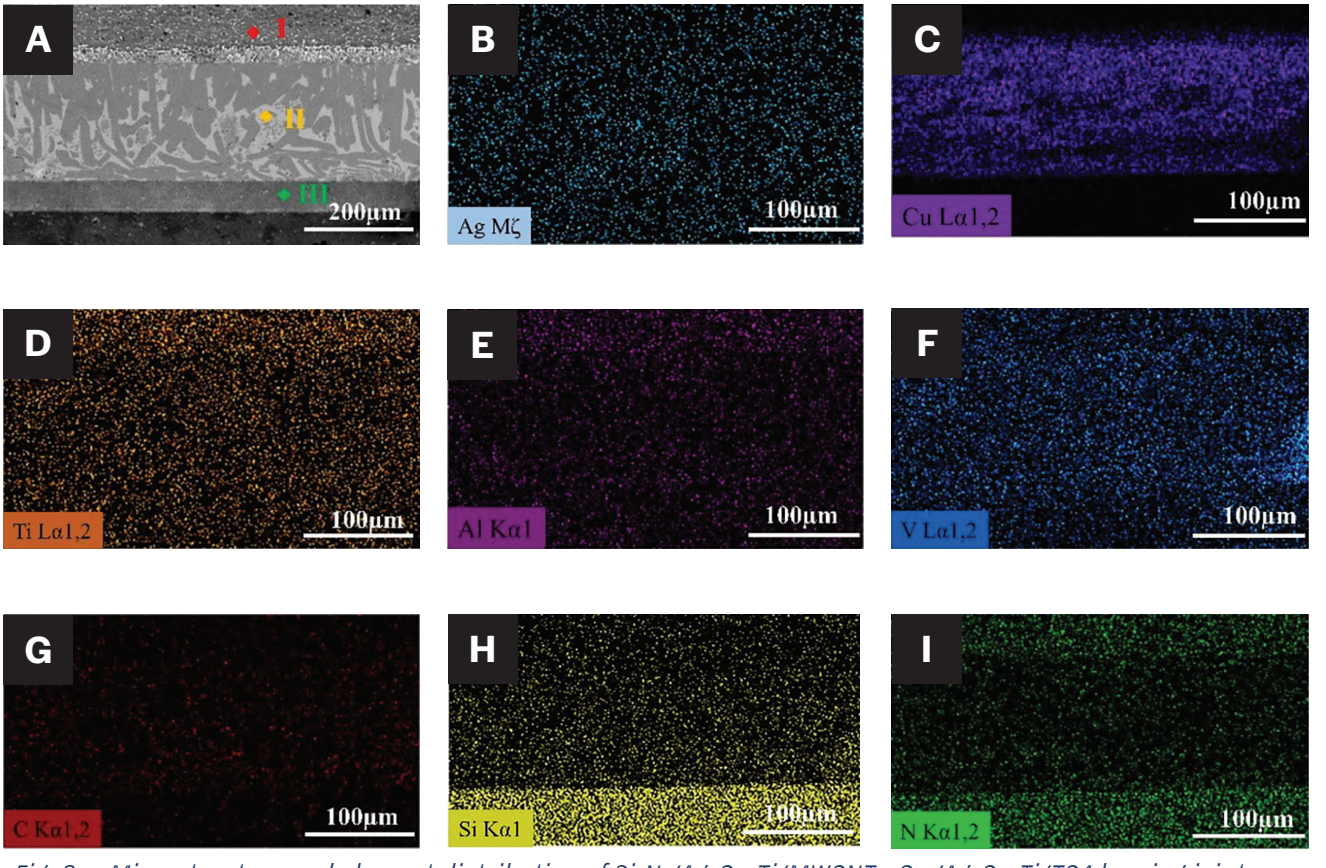

Fig. 8 — Microstructure and element distribution of Si_3N_4/Ag-Cu-Ti/MWCNTs-Cu_f/Ag-Cu-Ti/TC4 brazing joint (brazing temperature 880°C, holding time 10 min): A — The overall morphology of the joint; B — Ag; C — Cu; D — Ti; E — Al; F — V; G — C; H — Si; I — N.

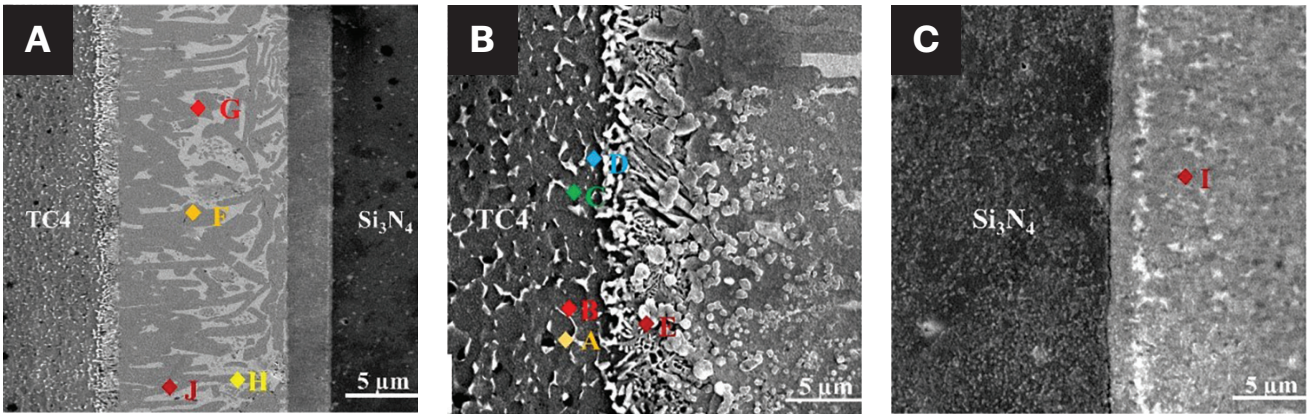

Fig. 9 — Interface microstructure of Si_3N_4/Ag-Cu-Ti/MWCNTs-Cu_f/Ag-Cu-Ti/TC4 joint in each region: A — Overall morphology; B — amplified portion of area (I); C — amplified part of area (III).

Table 1 — EDS Energy Spectrum Analysis Results of Elements at Each Point in Fig. 9 (at.-%)

Point	Ag	Cu	Ti	Al	V	Si	N	C	Phase
A	—	9.68	77.75	6.74	5.83	—	—	—	Diffusion layer
B	2.45	29.42	63.39	2.78	1.96	—	—	—	Ti_2Cu
C	0.58	47.42	49.17	1.68	1.15	—	—	—	TiCu
D	1.84	53.74	42.16	1.24	1.02	—	—	—	Ti_3Cu_4
E	2.87	74.87	18.62	1.35	0.67	—	—	1.62	TiCu4
F	2.56	94.64	2.58	—	—	—	—	—	Cu(s,s)
G	90.11	6.44	0.66	—	—	—	—	2.78	Ag(s,s)
H	63.46	34.79	1.75	—	—	—	—	—	Ag-Cu
I	1.02	9.11	44.04	0.62	0.38	17.93	26.91	—	TiN, Ti_5Si_3
J	3.65	4.42	46.57	—	—	—	—	45.36	TiC

cooling. At the same time, the molten brazing filler metal also cooled and solidified to form an Ag-Cu eutectic structure, with only a small amount of TiC compounds in the brazing layer, which improved the overall joint strength.

Finite Element Calculation Method

Based on the relationship between the thickness of the reaction layer and the width of the brazed joint, COMSOL Multiphysics finite element simulation software was used in this study to calculate the residual stress under different brazed joint widths and to investigate the effect of the reaction layer thickness on joint strength (Ref. 33). In this study, a geometric model of the assembly of Si_3N_4 ceramic and TC4 titanium alloy brazing samples was first established in a 1:1 ratio, and the constructed Si_3N_4/TC4 brazing geometric model meshed, as shown in Fig. 11. In analyzing residual stress distribution in Si_3N_4/TC4 brazed joints, the core research area was the composite brazed seam and its interface with the base material. Therefore, an ultra-fine mesh division method was applied to this area. The mesh of the composite brazed seam and its interface with the base material was set to be a free tetrahedral mesh, with a maximum element size of 0.7 mm, a minimum element size of 0.03 mm, a maximum element growth rate of 1.35, and a curvature factor of 0.3. To ensure both accurate calculation results and computational efficiency, relatively sparse mesh division methods

were applied to other areas of the TC4 titanium alloy and Si_3N_4 ceramic base materials. Similarly, the mesh of this area was also set to be a free tetrahedral mesh, with a maximum element size of 1.6 mm, a minimum element size of 0.2 mm, a maximum element growth rate of 1.45, and a curvature factor of 0.5. as shown in Figs. 11C and D. In this finite element analysis of residual stress distribution, the Si_3N_4/TC4 brazing geometric model had 12,309 mesh elements, with a minimum element quality of 0.2204 and an average element quality of 0.6427.

After solving with COMSOL software, the final result was obtained. Fig. 12 shows the calculated equivalent stress ofSi_3N_4/TC4 joints with MWCNTs-Cu_f composite intermediate layers brazed using different brazed joint widths. The MWCNTs-Cu_f composite intermediate layer with brazed joint widths of 0.1 mm,0.2 mm, 0.3 mm, and 0.4 mm were used. The von Mises stress on the TC4 side of the joint was very small, and it gradually increased as it approached the brazed layer, with a jump-like increase at the interface between TC4 and the brazed layer. The residual stress of the joint gradually decreased after reaching the maximum value at the interface between the brazed layer and the Si_3N_4 ceramic. The maximum residual stresses were 179 MPa,167 MPa, 134 MPa, and 146 MPa, respectively, and the residual stress reached its minimum value when the brazed joint width was 0.3 mm, which resulted in the highest joint strength. Compared to joints brazed directly with brazing materials, the peak residual stress of the brazed joints with an added composite intermediate layer was reduced by 38.2%. (The material properties and simulation boundary conditions are in the Appendix.)

Based on a 10-min insulation period, fracture morphology images (Fig. 13) and fracture surface EDS microstructures (Figs. 14A–C were obtained at different brazing temperatures, identifying three distinct fracture modes (Figs. 14D–F). When

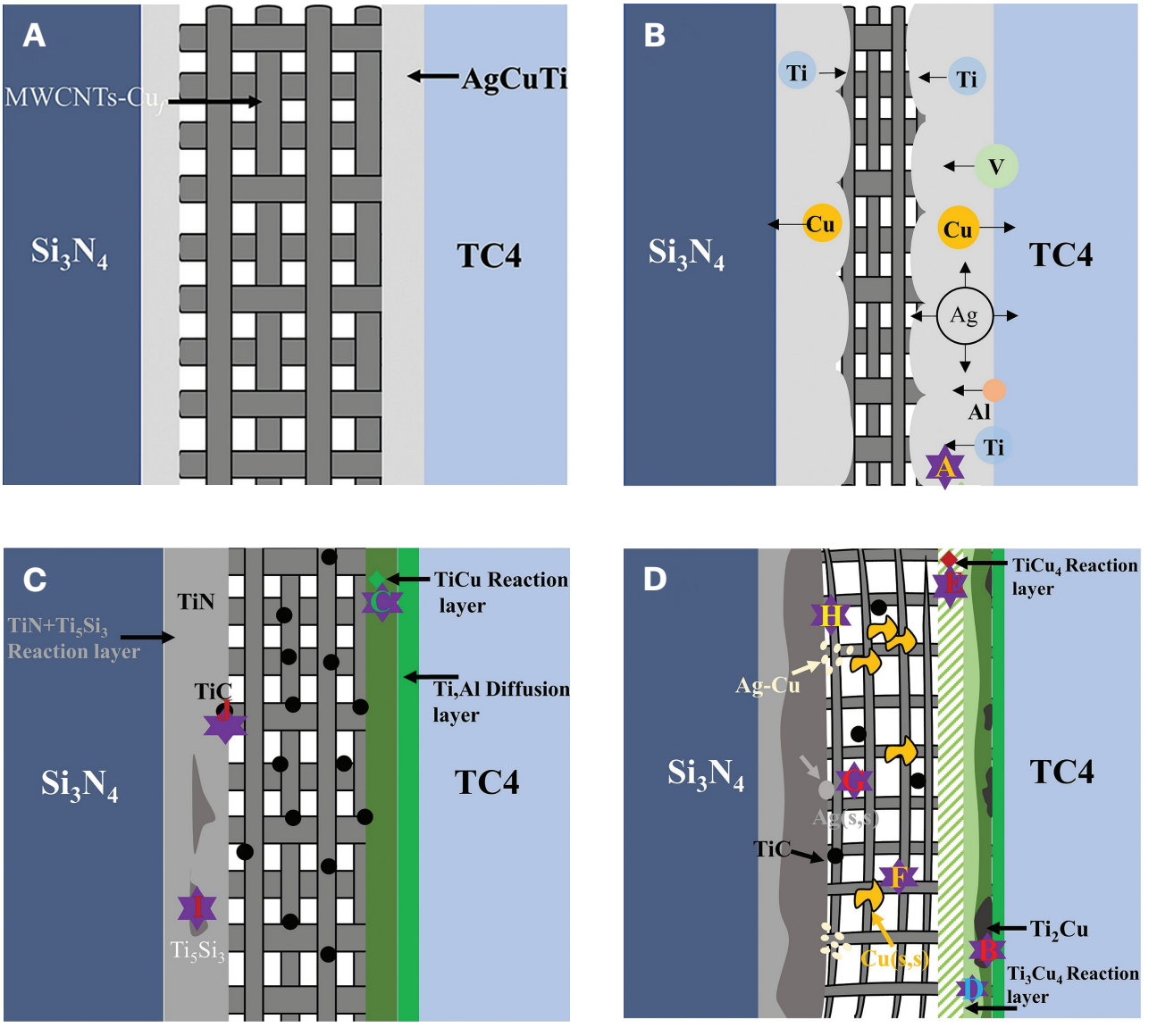

Fig. 10 — Schematic diagram of joint formation mechanism: A — Heating stage; B — the brazing filler metal melting stage; C — insulation stage; D — condensation stage (A-I is derived from the data in Table 1).

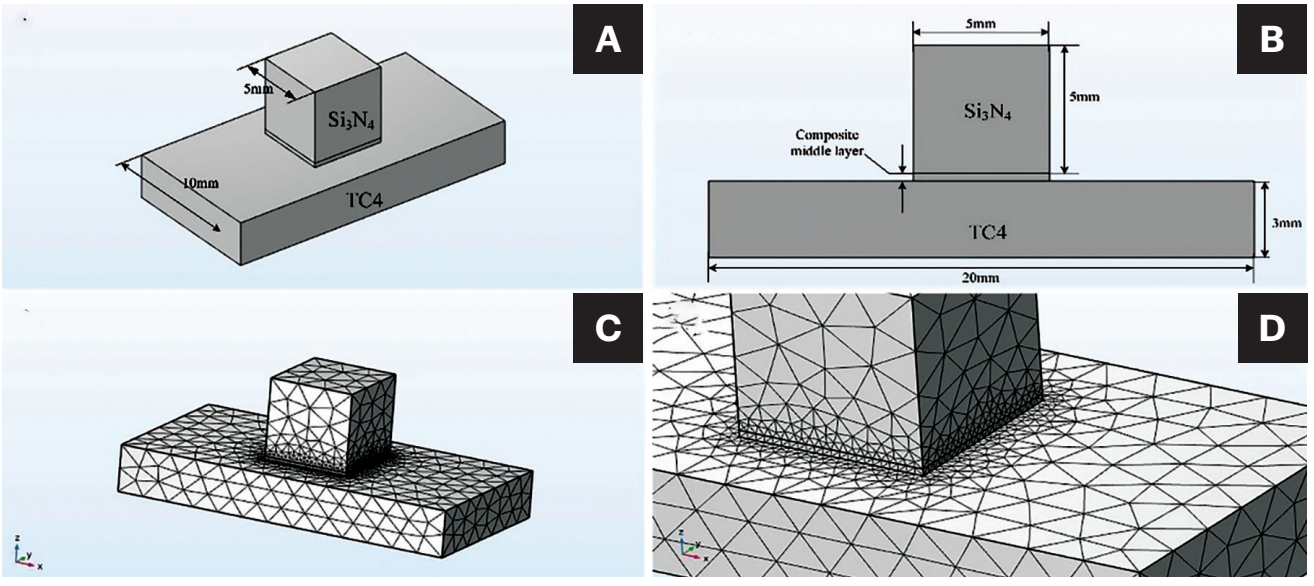

Fig. 11 — Geometric model and mesh partition diagram: A — Side view of the model; B — front view of the model; C — model meshing; D — partial enlarged view of model meshing.

the brazing temperature was 820°C, it was the first type of fracture mode, and cracks occurred from the interface and expanded along the interface. This was because the interface reaction layer was too thin, and the wettability of brazing filler metal to ceramic base metal was too poor. It lead to interface bonding failure and the lowest strength. When the brazing temperature was 850°C and 880°C, it was the second kind of fracture mode. Although this kind of fracture also occurred in the near-seam zone of ceramics, the crack did not only propagate in the near-seam zone of ceramics but passed through the brazing layer, and the fracture morphology had a small amount of brazing layer besides the ceramic base metal. The residual stress of the joint with this fracture mode is small. Therefore, under the action of external load, cracks occurred at the maximum stress of the joint and propagated along the brazing seam and finally broke. The joint strength of this fracture mode was higher. When the brazing temperature was further increased to 910°C, the third type of fracture mode occurred near the seam zone of ceramics, and the fracture path was arched. The interface adhesion between the ceramic and brazing filler metal layer was strong. Still, the difference in thermal expansion coefficients between the ceramic and metal brazing filler layer lead to axial tensile stress on ceramic base metal near the brazing filler metal layer during cooling. The maximum value occurred at the edges and corners of contact between the ceramic and brazing filler metal layer, so residual stress was difficult to release. Therefore, under the action of external load, cracks occurred and propagated at the edges and corners of the contact between ceramics and the brazing filler metal and finally showed an arched fracture path, resulting in low joint strength.

Through the above analysis, this paper summarizes the strengthening mechanism of composite interlayer: Firstly, the excellent plastic deformation ability and porous structure of foam copper as an intermediate layer in assisting brazing result in lower strain energy at the joints (Ref. 34) reduces residual stresses generated at the joint interface. Additionally, the carbon nanotubes deposited on its surface act as a barrier, preventing direct contact between Cu elements and the brazing filler metal at high temperatures, thus inhibiting their dissolution and diffusion. Therefore, throughout the brazing process, foam copper can maintain its porous scaffold structure, effectively mitigating the occurrence of collapse phenomena. This ensures the foam copper can uniformly disperse Cu (s,s) within the joint after cooling and solidification. Furthermore, the porous nature of foam copper allows the filling metal to occupy its voids, increasing the contact area between the filling metal and the intermediate layer. After cooling, Cu (s,s) distributes more evenly in the joint, resulting in refined microstructures. Secondly, the main issue with brazing filler metal to ceramic is the significant difference in the coefficient of thermal expansion between the base materials, leading to residual stresses during the cooling process. According to empirical formulas based on the mixture law, the coefficient of thermal expansion for Ag-Cu-Ti active filler metal is calculated to be 18.07×0^{-6}/K, which differs greatly from that of Si_3N_4 ceramic (3.2×10^{-6}/K). Adding carbon nanotubes can leverage their low coefficient of thermal expansion, reducing the joint's overall coefficient of thermal expansion. This effectively mitigates the difference in thermal expansion coefficients between Si_3N_4 ceramic and the joint, reducing residual stresses at the joint interface. Additionally, carbon nanotubes' extremely low coefficient of thermal expansion can generate high-density dislocations during brazing cooling, thereby inducing dislocation strengthening through slip bands (Ref. 35). According to the Orowan strengthening mechanism (Refs. 36, 37), MWCNTs act as second-phase particles belonging to non-deformable particles. When dislocation lines encounter them, they are bent around the NWCNTs due to obstruction. With increasing external stress, the bending intensifies until dislocations around the carbon nanotube particles meet and cancel out at the meeting point, leaving a dislocation loop around the MWCNTs. The entire process requires additional work, and

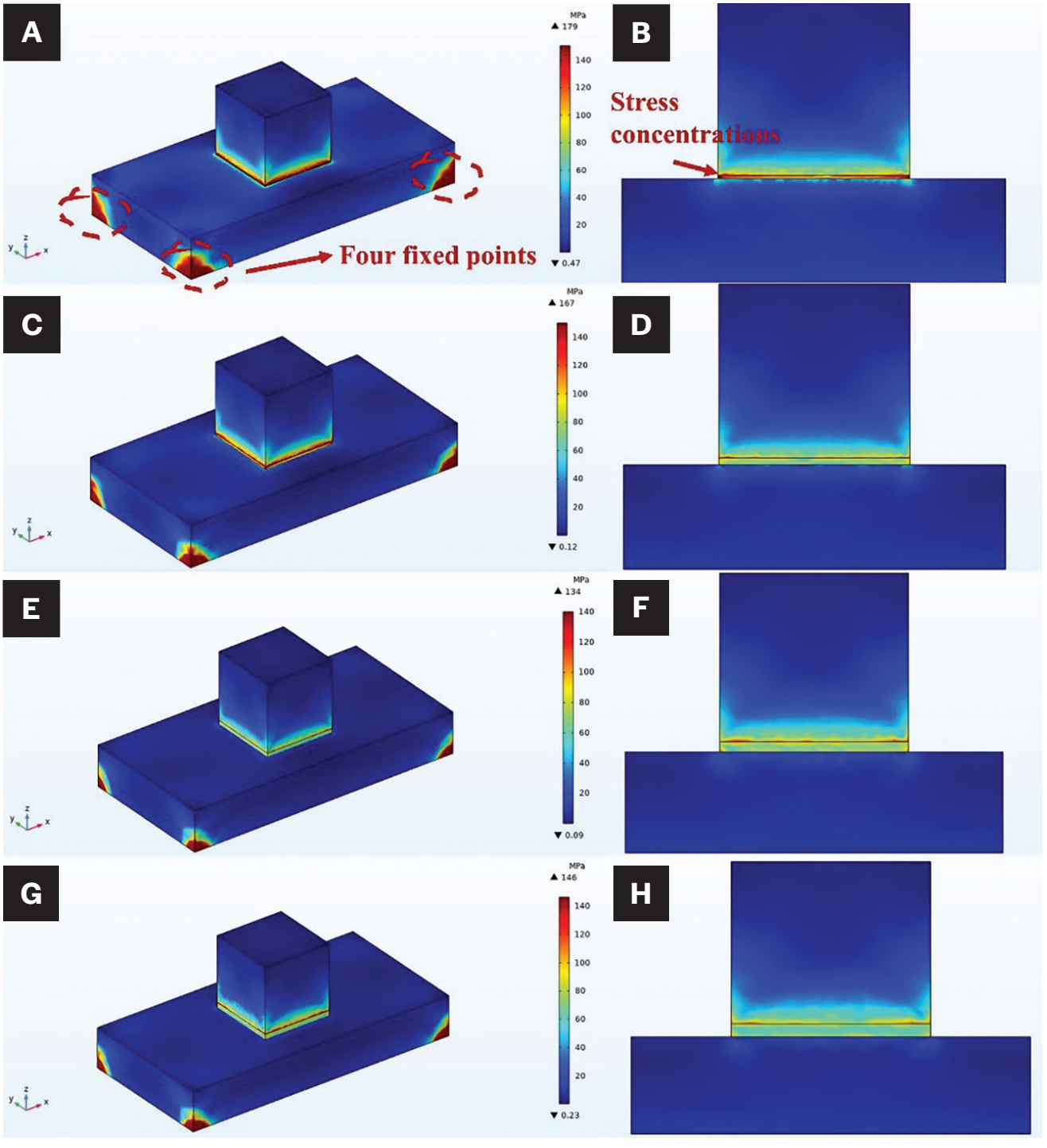

Fig. 12 — Equivalent stress distribution of Si_3N_4/TC4 joints brazed based on MWCNTs-Cu_t composite interlayer with different brazing widths: A–B — 0.1 mm; C–D — 0.2 mm; E–F — 0.3 mm; G–H — 0.4 mm.

the dislocation loop also hinders the movement of subsequent dislocations, leading to an increase in joint strength. Furthermore, the Orowan strengthening effect of carbon nanotubes is related to their diameter and spacing; the larger the diameter and the smaller the spacing, the more pronounced the Orowan strengthening effect. Moreover, according to the Hall-Petch theory (Ref. 38), when the material-to-surface area ratio is larger, the surface activity is greater, and the adsorption capacity is better. The good adsorption capacity of carbon nanotubes can adsorb Ti elements during the brazing reaction, thereby partially inhibiting the formation of Ti-Cu brittle compounds. The growth of the Ag-Cu eutectic structure requires overcoming interfacial free energy. At the same time, MWCNTs have a higher interfacial free energy, which can effectively inhibit the

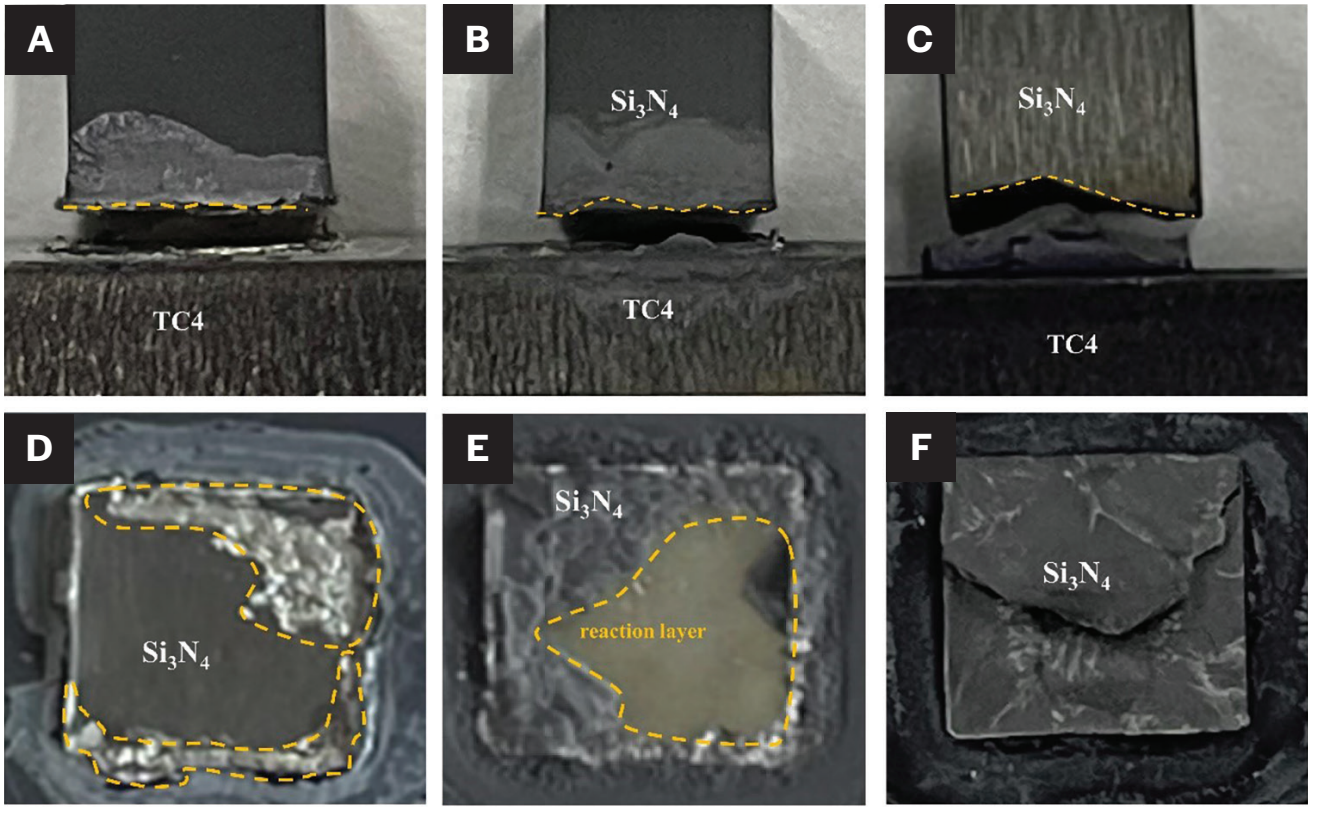

Fig. 13 — Sketch diagram of fracture morphology, fracture path of a joint under different brazing temperatures at 10 min holding time: A, D — 820°C; B, E — 880°C; C, F — 910°C.

Table 2 — EDS Energy Spectrum Analysis Results of Elements at Each Point in Fig. 14 (at.-%)

Point	Si	N	Ti	Cu	Ag	Al	C	O	Phase
A	37.45	49.65	—	—	—	—	7.27	5.63	Ceramic matrix
B	36.46	49.39	—	—	—	2.54	6.58	5.03	Ceramic matrix
C	18.57	11.54	41.77	7.69	0.88	7.94	5.23	6.38	Ceramic reaction layer
D	—	—	56.61	10.21	4.97	1.89	26.32	—	Brazed layer
E	15.31	12.58	45.66	8.32	2.38	3.69	2.38	9.68	Ceramic reaction layer

growth of the eutectic structure and refine the microstructure. According to the Hall-Petch formula: $\Delta\sigma_{Hall\text{-}petch} = Kd^{-½}$ (where K is a constant; d is the grain size in micrometers), the finer the grains, the higher the strength. A refined microstructure implies the presence of more grain boundaries, which can effectively prevent the generation of dislocations during brazing, thereby significantly enhancing the strength of the joint.

Conclusion

In this paper, the MWCNTs-Cu_f composite interlayer was prepared by electrophoretic deposition, and the best process of electrophoretic deposition was screened out. The effects of brazing temperature and holding time on the microstructure and shear strength of the joint were discussed in depth. The joint formation mechanism and fracture mode were analyzed, and the strengthening mechanism of

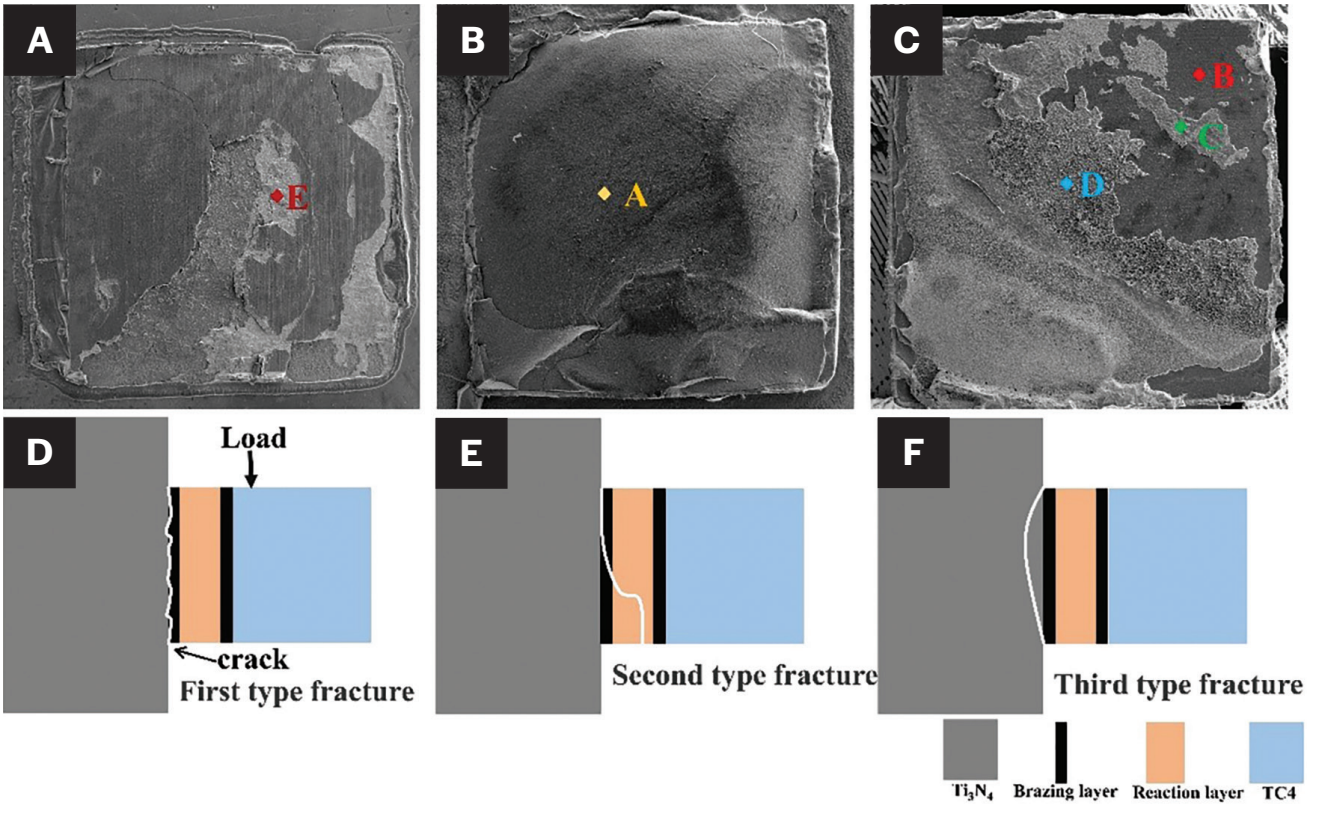

Fig. 14 — Fracture surface morphology diagrams and three types of fracture modes: A, D — 820°C; B, E — 880°C; C, F — 910°C (A-E is derived from the EDS data in Table 2).

MWCNTs and copper foam on brazed joints was clarified. The main conclusions are as follows:

1. When the concentration of MWCNTs was 0.3 mg/mL, the concentration of dimethyl diallyl ammonium chloride was 0.6 mg/mL, the deposition voltage was 120 V, and the deposition time was 20 min, the MWCNTs were deposited on the copper foam uniformly and densely. The optimum brazing parameters are a brazing temperature of 880°C and holding time of 10 min. The shear strength of the joint can reach 96.23 MPa, which is 78.2% and 44.7% higher than that of the joint with only Ag-Cu-Ti active filler metal and foam copper interlayer, respectively.

2. The porous structure and excellent plasticity of copper foam can enhance the contact area between copper foam and brazing filler metal, and the small strain energy can reduce the residual stress. The deposition of MWCNTs generated by electrophoresis on the surface of copper foam blocks the dissolution of Cu in copper foam to maintain the three-dimensional skeleton structure after brazing, giving full play to the porous structure and excellent plastic deformation characteristics of copper foam. The ratio of elements in brazing filler metal can remain unchanged so that the residual stress of the joint can be effectively relieved, and the shear strength can be improved.

3. When the width of the composite brazing seam is 0.3 mm, the residual stress reaches the minimum value of 134 MPa. Compared with the direct brazing of Si_3N_4/TC4 joint with Ag-Cu-Ti active brazing filler metal, the residual stress of the joint is reduced by 38.2% by adding a MWCNTs-Cu_f composite interlayer, which effectively relieves the residual stress of the brazing seam.

Authors' Contributions

Binbin Li conducted the experiment and numerical modeling. Binbin Li led data processing and manuscript preparation with contributions from all authors.

References

1. Guo, C., Fang, Y., and Laifei, C. 2021. In situ growth of single crystal Si_3N_4 nanowire foam with good wave-transparency and heat insulation performance. *Composites Part B: Engineering* 224(11): 109129. DOI: 10.1016/j.compositesb.2021.109129

2. Nag, A., Ramachandra Rao, R., and Panda, P. K. 2021. High temperature ceramic radomes (HTCR) - A Review. *Ceramics International* 47(15): 20793–20806. DOI: 10.1016/j.ceramint.2021.04.203

3. Wang, K., Liu, R., and Xu, H. 2022. High-strength and wave-transmitting Si_3N_4-Si_2N_2O-BN composites prepared using selective laser sintering. *Ceramics International* 48(14): 20126–20133. DOI: 10.1016/j.ceramint.2022.03.291

4. Clemens, H., and Mayer, S. 2013. Design, processing, microstructure, properties, and applications of advanced intermetallic TiAl alloys. *Advanced Engineering Materials* 15(4): 191–215. DOI: 10.1002/adem.201200231

5. Qin, W., Lin, N., Jin, F., and Huang, D. 2024. Effects of cementing matrix characteristics and particle size on the adhesion rule and mechanical properties of cemented granular materials. *Construction*

and Building Materials 411(1): 134630. DOI: 10.1016/j.conbuildmat.2023.134630

6. De Santis, Y., Aloisio, A., Pasquale Pasca, D., Gavrić, I., and Fragiacomo, M. 2024. Mechanical characterization of soundproofed inclined screws connections. *Construction and Building Materials* 412(1): 134641. DOI: 10.1016/j.conbuildmat.2023.134641

7. Ouyang, Y., and Chen, C. 2022. Research advances in the mechanical joining process for fiber reinforced plastic composites. *Composite Structures* 296(9): 115906. DOI: 10.1016/j.compstruct.2022.115906

8. Wei, K., Chen, Y., Li, M., and Yang, X. 2018. Strength and failure mechanism of composite-steel adhesive bond single lap joints. *Advances in Materials Science and Engineering* 2018: 1–10. DOI: 10.1155/2018/5810180

9. Liu, Y., Zhuang, W., and Wu, S. 2020. Damage to carbon fibre reinforced polymers (CFRP) in hole-clinched joints with aluminium alloy and CFRP. *Composite Structures* 234(2): 111710. DOI: 10.1016/j.compstruct.2019.111710

10. Liu, J., Zhang, J., Zhang, M., Wang, K., Zhang, A., Xiao, A., and Mao, C. 2023. Finite element analysis and experimental verification of residual stress in brazed diamond with Ni-Cr filler alloy. *Diamond and Related Materials* 139(11): 110350. DOI: 10.1016/j.diamond.2023.110350

11. Shu, X., Li, K., Li, Y., Xiong, Z., Huang, Y., and Li, S. 2022. Experimental investigation on brazing residual stress distribution in 304 L stainless steel core plate. *Journal of Constructional Steel Research* 193(6): 107257. DOI: 10.1016/j.jcsr.2022.107257

12. Yi, R., Chen, C., Shi, C., Li, Y., Li, H., and Ma, Y. 2021. Research advances in residual thermal stress of ceramic/metal brazes. *Ceramics International* 47(15): 20807–20820. DOI: 10.1016/j.ceramint.2021.04.220

13. Han, G. H., Bian, H., Zhao, H. Y., Song, X. G., Li, Y., Liu, D., Cao, J., and Feng, J. C. 2018. Interfacial microstructure and mechanical properties of TZM alloy and ZrC particle reinforced tungsten composite joint brazed using Ti-61Ni filler. *Journal of Alloys and Compounds* 747(5): 266–275. DOI: 10.1016/j.jallcom.2018.02.258

14. Han, G. H., Wang, Y. F., Zhao, H. Y., Song, X. G., Cao, J., and Feng, J. C. 2017. Vacuum brazing of TZM alloy to ZrC particle reinforced W composite using Ti-28Ni eutectic brazing alloy. *International Journal of Refractory Metals and Hard Materials* 69(12): 240–246. DOI: 10.1016/j.ijrmhm.2017.08.019

15. Sun, Z., Chen, X., Zhang, B., Bai, Y, J., and Zhang, L. X. 2022. Study on 3-dimensional graphene sponge reinforced C/C composites-TiAl alloy brazed joints. *Materials Science and Engineering: A* 839(4): 142832. DOI: 10.1016/j.msea.2022.142832

16. Song, X. G., Cao, J., Wang, Y. F., and Feng, J. C. 2011. Effect of Si_3N_4-particles addition in Ag-Cu-Ti filler alloy on Si_3N_4/TiAl brazed joint. *Materials Science and Engineering: A* 528(15): 5135–5140. DOI: 10.1016/j.msea.2011.03.032

17. Bridges, D., Ma, C., Zhang, S., Xue, S., Feng, Z., and Hu, A. 2018. Diffusion and wetting behaviors of Ag nanoparticle and Ag nanowire pastes for laser brazing of Inconel 718. *Welding in the World* 62(1): 169–176. DOI: 10.1007/s40194-017-0526-x

18. Bridges, D., Xu, R., and Hu, A. 2019. Microstructure and mechanical properties of Ni nanoparticle-bonded Inconel 718. *Materials & Design* 174(7): 107784. DOI: 10.1016/j.matdes.2019.107784

19. Ba, J., Lin, J., Wang, H., Qi, B., Zhong, Z., Wang, Z., Ma, Q., Qi, J., Cao, J., and Feng, J. 2018. Carbon nanotubes-reinforced Ni foam interlayer for brazing SiO_2-BN with Ti6Al4V alloy Using TiZrNiCu brazing alloy. *Ceramics International* 44(4): 3684–3691. DOI: 10.1016/j.ceramint.2017.11.136

20. Li, S., Du, D., Jiu, Y., Qin, J., Liu, Q., and Long, W. 2022. Brazing of C/C composite and TiAl alloy using TiNiSi filler metal added Cu interlayer. *Journal of Materials Engineering and Performance* 31(2): 1277–1284. DOI: 10.1007/s11665-021-06251-9

21. Yang, J. H., Zhang, L. X., Sun, Z., and Feng, J. C. 2019. A novel composite interlayer assembled for C/SiC-GH99 brazed joints. *Journal of Manufacturing Processes* 38(2): 543–548. DOI: 10.1016/j.jmapro.2019.01.030

22. Sun, Z., Zhang, L. X., Chang, Q., Zhang, Z. H., Hao, T. D., and Feng, J. C. 2018. Active brazed Invar-SiO_{2f}/SiO_2 joint using a low-expansion composite interlayer. *Journal of Materials Processing Technology* 255(5): 8–16. DOI: 10.1016/j.jmatprotec.2017.11.058

23. Brochu, M., Pugh, M. D., and Drew, R. A. L. 2004. Brazing silicon nitride to an iron-based intermetallic using a copper interlayer. *Ceramics International* 30(6): 901–910. DOI: 10.1016/j.ceramint.2003.10.011

24. Shirzadi, A. A., Zhu, Y., and Bhadeshia, H. K. D. H. 2008. Joining ceramics to metals using metallic foam. *Materials Science and Engineering: A* 496(1–2): 501–506. DOI: 10.1016/j.msea.2008.06.007

25. Gupta, N., Gupta, S. M., and Sharma, S. K. 2019. Carbon nanotubes: synthesis, properties and engineering applications. *Carbon Letters* 29(5): 419–447. DOI: 10.1007/s42823-019-00068-2

26. Moghaddari, M., Yousefi, F., Aparicio, S., and Hosseini, S. M. 2020. Thermal conductivity and structuring of multiwalled carbon nanotubes based nanofluids. *Journal of Molecular Liquids* 307(6): 112977. DOI: 10.1016/j.molliq.2020.112977

27. Takakura, A., Beppu, K., Nishihara, T., Fukui, A., Kozeki, T., Namazu, T., Miyauchi, Y., and Itami, K. 2019. Strength of carbon nanotubes depends on their chemical structures. *Nature Communications* 10(1): 3040. DOI: 10.1038/s41467-019-10959-7

28. Wang, Z., Wang, G., Li, M., Lin, J., Ma, Q., Zhang, A., Zhong, Z., Qi, J., and Feng, J. 2017. Three-dimensional graphene-reinforced Cu foam interlayer for brazing C/C composites and Nb. *Carbon* 118(7): 723–730. DOI: 10.1016/j.carbon.2017.03.099

29. Hou, P. X, Liu, C., and Cheng, H. M. 2008. Purification of carbon nanotubes. *Carbon* 46(15): 2003–2025. DOI: 10.1016/j.carbon.2008.09.009

30. Chen, X. H., Cheng, F. Q., Li, S. L., Zhou, L. P., and Li, D. Y. 2002. Electrodeposited nickel composites containing carbon nanotubes. *Surface and Coatings Technology* 155(2–3): 274–278. DOI: 10.1016/S0257-8972(02)00118-4

31. Lemusruiz, J., Leonpatino, C., and Aguilarreyes, E. 2006. Interface behaviour during the self-joining of Si_3N_4 using a Nb-foil interlayer. *Scripta Materialia* 54(7): 1339–1343. DOI: 10.1016/j.scriptamat.2005.12.014

32. Zhang, J., Guo, Y. L., Naka, M., and Zhou, Y. 2008. Microstructure and reaction phases in Si_3N_4/Si_3N_4 joint brazed with Cu-Pd-Ti filler alloy. *Ceramics International* 34(5): 1159–1164. DOI: 10.1016/j.ceramint.2007.02.006

33. Zhang, J., He, Y. M., Sun, Y., and Liu, C. F. 2010. Microstructure evolution of Si_3N_4/Si_3N_4 joint brazed with Ag-Cu-Ti+SiCp composite filler. *Ceramics International* 36(4): 1397–1404. DOI: 10.1016/j.ceramint.2010.02.010

34. Hasanzadeh, R., and Moradian, M. 2022. Recent developments in research on porous metals and foamed metals. *Metals* 12(9): 1486. DOI: 10.3390/met12091486

35. He, Y., Xu, H., Liu, Y., Chen, Y., and Ji, Z. 2022. Strengthening mechanism of B_4C@APC/Al matrix composites reinforced with bimodal-sized particles prepared by hydrothermal carbonized deposition on chips. *Journal of Materials Science & Technology* 123(10): 60–69. DOI: 10.1016/j.jmst.2022.01.012

36. Hadadzadeh, A., Baxter, C., Amirkhiz, B. S. and Mohammadi, M. 2018. Strengthening mechanisms in direct metal laser sintered $AlSi_{10}Mg$: Comparison between virgin and recycled powders. *Additive Manufacturing* 23(10): 108–120. DOI: 10.1016/j.addma.2018.07.014

37. Lee, T. J., and Kim, W. J. 2020. Microstructure and tensile properties of magnesium nanocomposites fabricated using mag-

nesium chips and carbon black. *Journal of Magnesium and Alloys* 8(3): 860–872. DOI: 10.1016/j.jma.2020.05.007

38. Tsao, L. C., Huang, C. H., Chung, C. H., and Chen, R. S. 2012. Influence of TiO_2 nanoparticles addition on the microstructural and mechanical properties of Sn0.7Cu nano-composite solder. *Materials Science and Engineering: A* 545(5): 194–200. DOI: 10.1016/j.msea.2012.03.025

Appendix: Material Properties and Boundary Conditions for the Simulation Section

Material Parameter Settings

For the determination of thermophysical parameters of composite braze joints, according to the homogenization theory of composite materials, the empirical formula of

Table 3 — Thermophysical Parameters of Ag-Cu-Ti Brazing Material and Cu (Ref.4)

Material	T (°C)	K (GPa)	G (GPa)	α ($10^{-6}K^{-1}$)	σ_s (MPa)
Ag-Cu-Ti	20	121.7	36.7	19.0	230
	200	109.5	33.0	19.7	170
	400	97.3	29.4	20.2	98
	600	81.5	24.6	20.5	25
	800	70.6	21.3	21.0	20
Cu	20	137.8	45.9	16.5	65
	200	122.2	40.7	17.2	60
	400	111.1	37.0	17.8	45
	600	66.7	22.2	19.4	30
	800	44.4	14.8	20.5	20

Table 4 — Thermophysical Parameters of Composite Braze Joint

	20°C	200°C	400°C	600°C	800°C
K_e/GPa	121.93	109.71	97.56	86.62	75.34
G_e/GPa	36.84	33.16	29.48	26.18	22.83
$\alpha_e/10^{-6}K^{-1}$	18.95	19.65	20.15	20.37	20.74
E_e/GPa	100.41	90.39	80.36	71.37	62.23
$\rho_e/g{\cdot}cm^{-3}$			9.49		
$\lambda/W{\cdot}(m{\cdot}K)^{-1}$			400		
$c/J{\cdot}(kg{\cdot}K)^{-1}$			24.98		

Table 5 — Thermophysical Parameters of Si_3N_4 Ceramics and TC4 (Refs. 5 and 6)

Materials	Temperature (°C)	Elastic Modulus (GPa)	Poisson's Ratio	Coefficient of Linear Expansion (10^{-6}/K)	Density (g/cm³)	Specific Heat Capacity (J·kg·K)	Thermal Conductivity (W·m⁻¹·K⁻¹)
Si_3N_4	—	320	0.25	3.28	3.19	711.8	12.6
TC4	200	109.8	—	9.9	—	1003	126
	400	99.9	0.34	10.8	4.51	1080	138
	600	89.9	—	11.3	—	1162	140
	800	79.9	—	11.5	—	1240	143

mixing law is adopted for the thermophysical parameters of some composite materials in most studies:

$$P = P_m(1 - V_{re}) + P_r V_{re} \tag{1}$$

where P is the properties of composites, P_m is the properties of the matrix material, V_{re} is the volume fraction of the reinforced phase in the composite material, and P_{re} is the Enhanced phase performance.

In practice, the empirical formula of mixing law cannot reflect the change of stress and strain of the reinforcing phase in matrix material, so it is not suitable for calculating the mechanical properties of complex composite braze joints, and it is easy to produce large errors to affect the calculation results. Therefore, based on the Mori-Tanaka model (Refs. 1, 2), a method for estimating the macroscopic equivalent properties of two microstructure composites is proposed, and the volume confinement modulus and shear confinement modulus are introduced:

$$\frac{1}{K_e + K^*} = \frac{\varphi_{cl}}{K_{cl} + K^*} + \frac{\varphi_s}{K_s + K^*} \tag{2}$$

$$\frac{1}{G_e + G^*} = \frac{\varphi_{cl}}{G_{cl} + G^*} + \frac{\varphi_s}{G_s + G^*} \tag{3}$$

where K_e is the bulk modulus (GPa) of the composite braze joint, K_{cl} is the bulk modulus (GPa) of the MWCNTs-Cu_f composite interlayer, K_s is the bulk modulus (GP) of the Ag-Cu-Ti brazing filler material, φ_{cl} is the volume fraction of the MWCNTs-Cu_f composite intermediate layer in the composite braze joint, φ_s is the porosity of copper foam, G_e is the shear modulus (GPa) of the composite braze joint, G_{cl} is the shear modulus (GPa) of MWCNTs-Cu_f composite interlayer, and G_s is the shear modulus (GPa) of the Ag-Cu-Ti brazing filler material. K^* and G^* can be represented as:

$$K^* = \frac{4(K_s G_{cl} - K_{cl} G_s)}{3(K_s - K_{cl}) + 4(G_s - G_{cl})} \tag{4}$$

$$G^* = \frac{6G_s(K_s + 2G_s)}{9K_s + 8G_s} \tag{5}$$

According to the relationship between elastic modulus, Poisson's ratio, bulk modulus, and shear modulus, it can be obtained:

$$E_e = \frac{9K_e G_e}{3K_e + G_e} \tag{6}$$

$$\gamma_e = \frac{3K_e - 2G_e}{6K_e + 2G_e} \tag{7}$$

where E_e is the modulus of elasticity (GPa) of the composite braze joint, and γ_e is the Poisson's ratio of composite braze seams.

Because Ag-Cu-Ti filler metal and MWCNTs-Cu_f composite interlayer are isotropic, and the interface bonding between the two phases is good at high temperatures, it conforms to the Kerner model (Ref. 3). Therefore, the expansion coefficient of the composite drill stitch is expressed as:

$$\alpha_e = \varphi_{cl}\alpha_{cl} + \varphi_s\alpha_s + \left[\frac{4G_s}{K_c}\right] \left[\frac{\varphi_{cl}(K_c - K_{cl})(K_c - K_{cl})}{4G_s + 3K_{cl}}\right] \tag{8}$$

where E_e is the linear expansion coefficient of the MWCNTs-Cu_f composite intermediate layer, α_s is the linear expansion coefficient (K^{-1}) of the Ag-Cu-Ti brazing filler material, and

K_c is the Hashin bulk modulus coefficient (Ref. 2) of the composite braze joint, the expression of which is:

$$K_c = \frac{\frac{\varphi_{cl}K_{cl}}{3K_{cl}+4G_s} + \frac{\varphi_s K_s}{3K_s+4G_s}}{\frac{\varphi_{cl}}{3K_{cl}+4G_s} + \frac{\varphi_s}{3K_s+4G_s}} \quad (9)$$

Therefore, the mechanical properties of the MWCNTs-Cu_f composite interlayer and Ag-Cu-Ti filler metal can be calculated based on the above-mentioned model. The mechanical properties of the composite brazing joint can be calculated. The equivalent elastic modulus, linear expansion coefficient, and Poisson's ratio of the composite brazing joint can be obtained based on the calculated mechanical properties of the MWCNTs-Cu_f composite interlayer and Ag-Cu-Ti filler metal.

The thermal physical parameters of the Ag-Cu-Ti brazing material and Cu are shown in Table 3. Additionally, the equivalent density (ρ), equivalent thermal conductivity (λ), and equivalent specific heat capacity (*c*) of the composite brazed joint are not affected by temperature. Due to the similar properties of foam copper and Ag-Cu-Ti brazing material and the high thermal conductivity of MWCNTs, calculations for the thermal physical parameters of the composite brazed joint can be directly performed using Equation 3, yielding results as shown in Table 4. The material supplier provides the thermal physical parameters of Si_3N_4 ceramics and TC4 titanium alloy, as indicated in Table 5.

Setting of Joint Boundary Conditions and Initial Conditions

Initial Conditions

During the heating and holding phases of the brazing process between Si_3N_4 ceramics and TC4, all three substrates remain in a free state, and stress only develops during the cooling stage when the brazing material solidifies. Therefore, only the cooling process is considered when calculating the residual stress distribution. The reference temperature for volume is set at 880°C. Under the brazing conditions of 880°C and 10 min holding time, Si_3N_4 ceramics do not undergo plastic deformation. Hence, only elastic deformation of the ceramics is considered in this calculation. Additionally, due to the high brazing temperature, the mechanical and physical properties of TC4 will undergo corresponding changes with increasing temperature. It is assumed that the physical and mechanical properties of Si_3N_4, the composite brazed joint, and TC4 are all isotropic.

Thermal Boundary Conditions

During the brazing process between Si_3N_4 ceramics and TC4, the overall sample size is relatively small and the cooling rate is slow. For ease of calculation, it can be assumed that the temperature within and outside the brazing sample is uniform and there is no temperature gradient. Therefore, based on actual experimental conditions, an initial temperature of 880°C was set for the overall sample, and a temperature curve was established, cooling at a rate of 5°C/min until reaching room temperature.

Mechanical Boundary Condition

In the actual brazing process, a certain pressure will be applied at the top to ensure the stability of the sample and tight contact between interfaces. In contrast, the bottom of the sample directly contacts the tubular furnace. Therefore, in setting the mechanical boundaries, fixed constraints were applied to the four points at the bottom of the sample to prevent any movement or rotation of the sample model during the cooling process.

During the brazing process of Si_3N_4/TC4 using an MWCNTs-Cu_f composite interlayer, the residual stresses in the joint are primarily influenced by the brazing temperature and cooling rate. Generally, rapid cooling rates result in higher residual stresses in the joint, adversely affecting brazing shear strength enhancement. Therefore, the process parameters adopted for this finite element analysis were as follows: an initial temperature of 880°C and a cooling rate of 5°C/min until reaching room temperature.

References

1. Gong, S., Li, Z., and Zhao, Y. Y. 2011. An extended Mori–Tanaka model for the elastic moduli of porous materials of finite size. *Acta Materialia* 59(17): 6820–6830. DOI: 10.1016/j.actamat.2011.07.041

2. Tsukamoto, H. 2010. A mean-field micromechanical model of thermal-ratcheting behavior in short fiber-reinforced metal matrix composites. *Acta Materialia* 58(10): 3709–3717. DOI: 10.1016/j.actamat.2010.03.008

3. Balch, D. K., Mortensen, A., Suresh, S., Shen, Y. L., Fitzgerald, T. J., and Michaud, V. J. 1996. Thermal expansion of metals reinforced with ceramic particles and microcellular foams. *Metallurgical and Materials Transactions A* 27(11): 3700–3717. DOI: 10.1007/BF02595462

4. Li, J. L., Xiong, J. T., and. Zhang, F. S. 2008. Transient liquid-phase diffusion bonding of two-dimensional carbon-carbon composites to niobium alloy. *Materials Science and Engineering: A* 483–484(6): 698–700. DOI: 10.1016/j.msea.2006.11.170

5. Chen, C., Liang, X., Luo, M., Zhou, S., Ji, J., Huang, Z., and Xu, M. 2019. Preparation and characterization of porous Si_3N_4-Bonded SiC ceramics and morphology change mechanism of Si_3N_4 whiskers. *Ceramics International* 45(5): 5922–5926. DOI: 10.1016/j.ceramint.2018.12.060

6. Zou, Z., Zeng, F., Wu, H., Liu, J., Li, Y., Gu, Y., Yuan, T., and Zhang, F. 2017. The joint strength and fracture mechanisms of TC4/TC4 and TA0/TA0 brazed with Ti-25Cu-15Ni braze alloy. *Journal of Materials Engineering and Performance* 26(5): 2079–2085. DOI:10.1007/s11665-017-2554-5

BINBIN LI (*bbli@nuaa.edu.cn*), **LIANGLIANG CAO**, **QIANLI LIU**, **JINGMIN GAO**, and **RUIBIN LI** are with the College of Materials Science and Technology, Nanjing University of Aeronautics and Astronautics, Nanjing, People's Republic of China.